Wavelength dependence of visible and near-infrared photorefraction and phase conjugation in $Sn_2P_2S_6$

Mojca Jazbinšek, Daniel Haertle, Germano Montemezzani, and Peter Günter

Nonlinear Optics Laboratory, Institute of Quantum Electronics, Swiss Federal Institute of Technology, CH-8093 Zurich, Switzerland

Alexander A. Grabar, Ivan M. Stoika, and Yulian M. Vysochanskii

Institute of Solid State Physics and Chemistry, Uzhgorod National University, 88 000 Uzhgorod, Ukraine

Received April 11, 2005; revised manuscript received June 4, 2005; accepted June 12, 2005

The photorefractive properties of $Sn_2P_2S_6$ crystals in the wavelength range from 633 to 1064 nm are investigated. Conventional yellow and modified brown crystals with a variation of nonstoichiometric defects are examined. Brown crystals respond much faster and exhibit substantially higher photorefractive gain than yellow crystals, up to 18 cm^{-1} at 780 nm and 8.5 cm^{-1} at 1064 nm. Ring-cavity self-pumped phase conjugation is demonstrated using both types of crystal. The phase-conjugate response of brown $Sn_2P_2S_6$ is 2 orders of magnitude faster than in yellow $Sn_2P_2S_6$ or Rh-doped $BaTiO_3$, with a grating recording time below 50 ms for 30 mW power at 860 nm. Various thresholding effects are analyzed to determine the optimal wavelength range for the two types of crystal. We find an optimum in the range of 650–950 nm for yellow and in the range of 850–1100 nm for brown $Sn_2P_2S_6$.

OCIS codes: 160.5320, 190.5040, 190.5330, 190.7070.

1. INTRODUCTION

Photorefractive materials have been studied intensively in the past few decades because of their utilization in a variety of applications.[1–3] Recently it has been of considerable interest to improve their response in the near-infrared wavelength range of widely available laser diodes. Unfortunately conventional photorefractive materials tend to be less sensitive in the near infrared and only a few materials have been shown to exhibit a substantial photorefractive response. These materials are semiconductor photorefractive crystals such as GaAs, InP, CdTe, GaP, CdS, which are relatively fast but have small nonlinearity and require high external electric fields, and semiconductor multiple quantum-well structures, where the interaction length is limited because of the small thickness.[3] On the other hand, among conventional photorefractive materials, reduced Rh-doped $KNbO_3$ (Ref. 4) and Rh-doped $BaTiO_3$ (Ref. 5) have been shown to exhibit a relatively large nonlinearity, but have a rather slow response. Rh:$BaTiO_3$ has been especially intensively optimized in the past years by many groups to obtain photorefractive gain values as large as $\Gamma = 23$ cm^{-1} at a light wavelength $\lambda = 1.06$ μm with a response time of 75 s at a light power of 20 W/cm^2.[6,7] Self-pumped phase conjugation in the near infrared is commonly obtained using Rh:$BaTiO_3$, but the response time is still of the order of 10 s at $\lambda = 1.06$ μm and 5 W/cm^2.[8]

Here we consider another near-IR-sensitive material, tin hypothiodiphosphate ($Sn_2P_2S_6$). In contrast to most conventional ferroelectrics that are insulators, $Sn_2P_2S_6$ has a smaller bandgap of 2.3 eV at room temperature that results in pronounced semiconductor features. The photorefractive response of $Sn_2P_2S_6$ is much faster than that of Rh:$BaTiO_3$ or Rh:$KNbO_3$, also without application of external fields. At $\lambda = 633$ nm and 1 W/cm^2 with conventional yellow $Sn_2P_2S_6$, the response time is of the order of 10 ms.[9] The measured gain coefficients were up to 7.5 cm^{-1} at $\lambda = 633$ nm (Refs. 9 and 10) and up to 6 cm^{-1} at $\lambda = 1.06$ μm, the latter obtained by using a focused laser beam with an intensity of ~ 50 W/cm^2 and preillumination.[11,12] With an external electric field, a gain factor of more than 15 cm^{-1} was achieved at $\lambda = 0.9$ μm.[13] A strong electron–hole competition has been observed in yellow $Sn_2P_2S_6$, which leads to transient behavior and decreases the gain in the steady state.[12]

Defect centers that are responsible for photorefraction in $Sn_2P_2S_6$ are not yet clearly identified; however, we consider various crystal types with respect to their characteristic properties as explained in the following. In crystals with pronounced electron–hole competition, which we call type I yellow $Sn_2P_2S_6$ crystals, the photorefractive gain is also sensitive to preillumination, and the exponential gain coefficient can increase by a factor of 2–3 after preexposure with white light.[12] The competition of two out-of-phase gratings in type I yellow $Sn_2P_2S_6$ crystals with different decay times results in splitting of the spectrum of the steady-state gain factor.[14] This leads to a specific dynamics of the self-pumped phase conjugation in a ring cavity with a high-index-contrast amplitude.[10] Different response characteristics were obtained in the so-called type II yellow $Sn_2P_2S_6$ crystals.[15] For these crystals no transient gain and preillumination influence were de-

tected. Recently, a brown modification of $Sn_2P_2S_6$ was obtained with improved gain of up to $\Gamma = 38\ cm^{-1}$ at $\lambda = 633$ nm and an even faster response.[16,17] In brown crystals, presumably with a variation of nonstoichiometric defects, the absorption is increased in the vicinity of the absorption edge that is additionally shifted toward longer wavelengths.[16] Brown $Sn_2P_2S_6$ crystals are also not sensitive to preillumination with white light and do not show a pronounced electron–hole competition. Self-pumped phase conjugation was demonstrated in brown $Sn_2P_2S_6$ at $\lambda = 780$ nm with a very fast response that is below 50 ms at 1 W/cm^2.[17]

In this paper we report on the wavelength dependence of photorefractive properties and self-pumped phase conjugation in both yellow type II and brown $Sn_2P_2S_6$ toward longer wavelengths up to $\lambda = 1.06\ \mu m$. We discuss the optimization of the phase-conjugate performance at different wavelengths considering absorption, photorefractive gain, intensity, dark conductivity, and the transmission of a phase-conjugation cavity. Thresholding behavior of the phase-conjugate reflectivity in $Sn_2P_2S_6$ is analyzed regarding ring-cavity losses, light intensity, and photorefractive coupling strength.

2. CRYSTAL PROPERTIES

$Sn_2P_2S_6$ crystals used in our measurements were grown by the chemical vapor transport reaction technique[18] that is schematically presented in Fig. 1. Several transport agents can be selected to grow $Sn_2P_2S_6$ by this technique: I_2, SnI_2, or SnI_4. The choice of the transport gas affects the growth speed and the stoichiometry level of the grown crystals. Conventional yellow crystals that we used in our experiments were grown employing SnI_4 as a transport gas. Modified brown crystals, presumably of a lower stoichiometry level,[16] were grown employing SnI_2 gas.

At room temperature $Sn_2P_2S_6$ has a ferroelectric monoclinic structure with point group m. We use a coordinate system with the z axis parallel to the crystallographic c axis, the y axis normal to the mirror plane, and the x axis normal to z and y[19]; the $Sn_2P_2S_6$ samples were oriented by x rays, cut along the x, y, and z axes, and polished normal to the z axis. Crystals were poled above the phase-transition temperature $T_c = 337$ K by applying an electric field of ~500 V/cm normal to the x faces and then slowly cooled down with the applied electric field. The main axis of the optical indicatrix at room temperature is rotated by ~43° at 633 nm, 46° at 780 nm, and 50° at 1064 nm around the y axis away from the x axis in the x,z plane.[19]

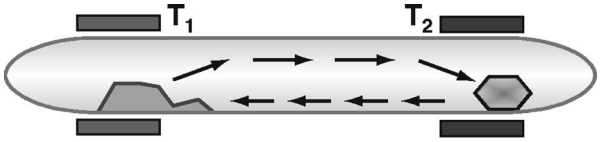

Transport gas	T_1 (K)	T_2 (K)	Color
I_2	900±10	840±10	orange
SnI_4	800±10	770±10	yellow
SnI_2	840±10	800±10	light-brown

Fig. 1. Scheme of the vapor transport growth of $Sn_2P_2S_6$.[18] High-purity stoichiometric amounts of the constituting elements are sealed into an evacuated quartz tube together with a transport gas. The tube is placed in a horizontal furnace with the temperature gradient between hot evaporation (T_1) and cold crystallization (T_2) zones. A transport gas replacement leads to variations in the growth speed and crystallization conditions due to the difference in the transport dynamics and the decomposition energy, and hence the crystal stoichiometry. This is usually manifested in the sample color varying from light yellow to orange or even a light-brown tone.

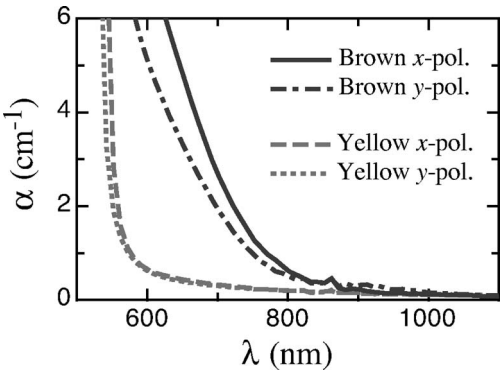

Fig. 2. Absorption spectra of yellow and brown $Sn_2P_2S_6$ crystals for light polarized along the x and y axes.

The optical absorption coefficients at room temperature were obtained from transmission measurements using a Perkin-Elmer λ9 spectrophotometer. Spectra were measured with light polarized along the x and y axes and analyzed taking into account the refractive-index dispersion[19] and multiple reflections at the surfaces. The yellow and brown $Sn_2P_2S_6$ crystals used in this measurement were, respectively, $z = 5.7$ mm and $z = 2.4$ mm thick. Figure 2 shows the absorption coefficients as a function of the light wavelength λ. An enhanced absorption band is revealed in the brown crystal. For example, at 633 nm the absorption coefficient α_x is increased from ~0.5 cm^{-1} in yellow $Sn_2P_2S_6$ to ~5.7 cm^{-1} in brown $Sn_2P_2S_6$, whereas at 1064 nm it is increased by less than 10% to ~0.1 cm^{-1}.

3. TWO-WAVE MIXING

All photorefractive experiments were performed at room temperature. The measurements were carried out at different wavelengths: $\lambda = 633$ nm (He–Ne laser, maximal cw power $P_{max} = 5$ mW), 780 nm (external-cavity diode laser, $P_{max} = 300$ mW, Rainbow Photonics AG, Zurich), 860 nm (Ti:sapphire laser, $P_{max} = 200$ mW), 980 nm (laser diode, $P_{max} = 100$ mW, Semiconductor Laser International), and 1064 nm (Nd:YAG laser, $P_{max} = 200$ mW). To avoid reflections and phase-conjugate feedback from affecting laser oscillation, a Faraday isolator was inserted in front of all the lasers used.

For the measurements of the two-beam coupling gain the usual experimental setup was used with the crystal x axis oriented in the incidence plane x,z and perpendicular to the bisector of the two incident beams. Both waves were extraordinary polarized in the plane of incidence. The yellow and brown $Sn_2P_2S_6$ crystals used for this measurement were, respectively, $z = 5.7$ mm and $z = 2.4$ mm thick. The intensity ratio of the pump wave to the weak

signal wave was at all the wavelengths high enough to neglect the pump-wave depletion. In this case the two-wave mixing exponential coefficient can be calculated as $\Gamma = 1/z \ln(I_{\text{signal with pump}}/I_{\text{signal without pump}})$. We have also checked experimentally with a configuration that would employ mainly the electro-optic coefficient r_{222} that is zero in $Sn_2P_2S_6$. The results have shown that an eventual contribution of the absorption gratings[20] can be neglected within our experimental accuracy. In both crystal types and for all investigated wavelengths, the weak signal beam was amplified if it was propagating toward the $+x$ direction in the incident x,z plane. Because of the positive sign of the corresponding electro-optic coefficient,[21] this implies that the dominant charge transport carriers are holes.[1–3]

Figure 3 shows the measured dependence of the two-wave mixing gain Γ on the grating spacing $\Lambda = \lambda/(2 \sin \theta)$, where 2θ is the external angle between the intersecting beams. Measurements at light wavelengths $\lambda = 780$ and 1064 nm are shown. Large values of the two-wave mixing gain coefficients are observed in the brown crystal, with a maximum of $\Gamma = 18\ \text{cm}^{-1}$ at 780 nm and $\Lambda_0 \simeq 1.5\ \mu$m, and $\Gamma = 8.5\ \text{cm}^{-1}$ at 1064 nm and $\Lambda_0 \simeq 2\ \mu$m. The corresponding response time τ_{twm} for an intensity of 0.2 W/cm^2 at 780 nm is approximately 15 ms, and 0.26 s at 1064 nm and 3.6 W/cm^2. In the yellow sample the measured gain coefficients are much lower (see Fig. 3), with a maximum of $\sim 2.5\ \text{cm}^{-1}$ at 780 nm and $\Lambda_0 \simeq 3\ \mu$m with the response time of approximately 0.2 s for an intensity of 0.2 W/cm^2. In both yellow and brown $Sn_2P_2S_6$ the response becomes faster at larger grating spacings, e.g., in the brown sample the response time at 780 nm and 0.2 W/cm^2 for grating spacings above 3 μm is shorter that 10 ms. This indicates that the Debye grating spacing Λ_0 corresponding to a maximal two-wave mixing gain is shorter than the diffusion length[1–3] in both yellow and brown crystal types.

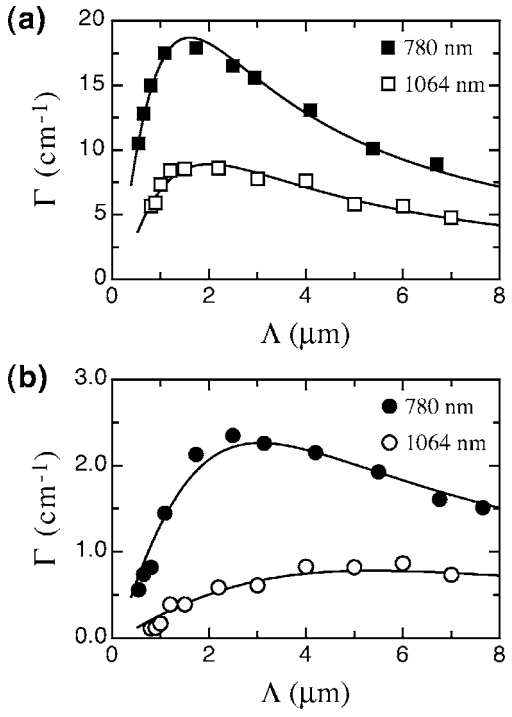

Fig. 3. Fringe spacing Λ dependence of two-beam coupling gain coefficient Γ at light wavelengths 780 nm with total input intensity $I = 0.2$ W/cm^2 and 1064 nm with $I = 3.6$ W/cm^2 in (a) brown $Sn_2P_2S_6$ and (b) yellow $Sn_2P_2S_6$. The solid curves are theoretical curves according to Eq. (1).

Table 1. Effective Electro-Optic Coefficients r^{eff} and Effective Concentration of Traps N_{eff} That Correspond to the Theoretical Curves of Fig. 3

$Sn_2P_2S_6$ Sample	λ (nm)	r^{eff} (pm/V)	N_{eff} (10^{16} cm^{-3})
Yellow	780	41±2	0.14±0.02
	1064	38±5	0.044±0.009
Brown	780	178±9	0.67±0.06
	1064	161±7	0.43±0.04

For the diffusion case and assuming an isotropic photoexcitation cross section, one obtains for the stationary two-wave mixing exponential gain coefficient within the weak probe beam approximation[22,23]

$$\Gamma = \frac{2\pi}{\lambda} n_S n_P^2 \cos \beta_{\text{P}} \frac{\hat{\mathbf{e}}_S \cdot \hat{\mathbf{e}}_P}{\cos \theta_S} r^{\text{eff}} E^{\text{SC}}, \tag{1}$$

where n_S and n_P are the refractive indices seen by the signal and the pump beam, β_{P} is the angle between the pump beam Poynting vector and the wave vector, θ_S the angle between the Poynting vector of the signal beam and the sample normal, $\hat{\mathbf{e}}_S$ and $\hat{\mathbf{e}}_P$ are the electric field unit vectors of the interacting beams, and r^{eff} is the effective electroptic coefficient. The steady-state space-charge electric field in the case of diffusion-dominated charge transport is given by

$$E^{\text{SC}} = \frac{E_D E_q}{E_D + E_q}, \tag{2}$$

where $E_D = (k_{\text{B}}T/e)(2\pi/\Lambda)$ is the diffusion electric field and $E_q = (e/\epsilon_{\text{eff}}\epsilon_0)(\Lambda/2\pi)N_{\text{eff}}$ is the trap-limiting field. Here k_{B} is the Boltzmann constant, T is the absolute temperature, e is the unit charge, ϵ_0 is the electric constant, ϵ_{eff} is the effective dielectric constant, and N_{eff} is the effective concentration of traps. For our geometry we assume $\cos \beta_{\text{P}} \simeq 1$ and $\hat{\mathbf{e}}_S \cdot \hat{\mathbf{e}}_P \simeq \cos 2\theta_S$. For the effective dielectric constant we take $\epsilon_{\text{eff}} \approx 300$ for brown samples and $\epsilon_{\text{eff}} \approx 230$ for yellow samples.[16] The refractive indices can be calculated using the Sellmeier model with the parameters given in Ref. 19 and taking into account the indicatrix rotation, which gives for our geometry approximately $n_S = n_P \approx 2.93$ at 780 nm and 2.84 at 1064 nm. The solid curves in Fig. 3 present the theoretical approximations according to Eq. (1). From the model parameters we can estimate the effective electro-optic coefficient r^{eff} and the effective concentration of traps N_{eff}. The obtained parameters are listed in Table 1. Because of the larger effective concentration of traps, the optimal coupling in brown $Sn_2P_2S_6$ is observed at smaller grating spacings than in yellow $Sn_2P_2S_6$. A lower gain obtained in yellow samples is mainly due to hole–electron compensation effects, which are not significant in brown samples.[16] The higher value obtained in brown $Sn_2P_2S_6$ is a result of a larger effective electro-optic coefficient. Even though in general the effective electro-optic coefficient is not expected to cor-

respond to one of the elements of the unclamped electro-optic tensor,[24] we have a surprisingly good correspondence with the directly measured electro-optic coefficient $r_{111}^{T}=(168\pm13)$ pm/V at $\lambda=780$ nm.[21] A slight decrease of r^{eff} with λ is also in agreement with the results of the direct measurements.[21] The decrease of the effective concentration of traps N_{eff} with λ confirms that more than one bandgap level is involved in photorefraction of $Sn_2P_2S_6$.

4. RING-CAVITY SELF-PUMPED PHASE CONJUGATION

The experimental setup for the ring-cavity self-pumped phase conjugation is depicted in Fig. 4. The light beams were polarized in the plane of the ring-cavity loop and almost parallel to the x axis in the crystal to use the largest electro-optic coefficient r_{111}. The external angle 2θ was adjusted at each laser wavelength approximately to the angle corresponding to the maximum measured two-wave mixing gain Γ (Fig. 3). The crystals were rotated by $\beta\approx45°-50°$ with respect to the incident beam to reduce the Fresnel losses. In these experiments a yellow crystal with dimensions $x\times y\times z=8.05$ mm $\times 8.91$ mm $\times 9.72$ mm and a brown crystal with $x\times y\times z=4.40$ mm $\times 5.68$ mm $\times 2.42$ mm were used. We coated the crystals with an approximately 100 nm thick Al_2O_3 layer to reduce the reflection losses by $\sim$50% at normal incidence in a wide wavelength range (800–1100 nm). The ring-cavity length was $\sim$40–45 cm and one of the mirrors in the cavity was vibrating to ensure that input beam 3 and feedback beam 1 were not coherent. In this case the reflection gratings created by pairs of beams (1,3), (2,4), (1,4), and (2,3) cannot be formed in the crystal. The generated phase-conjugated signal is then a result of the coupling via the transmission grating formed by incident beam 3 and its self-diffracted beam 4 as well by their feedback beams 1 and 2. The intensity of phase-conjugated wave 2 is measured by a photodiode placed after a beam splitter. The phase-conjugate reflectivity R is defined as the ratio between the measured intensity of the phase-conjugated wave 2 and input wave 3.

Figure 5 shows the time evolution of the phase-conjugate reflectivity R after the input beam 3 was turned on. In the beginning the phase-conjugated signal emerges from the noise gratings of the scattered input beam. After the external loop is restored, the desired transmission grating dominates and the phase-conjugated signal increases sharply and finally it saturates at its maximum

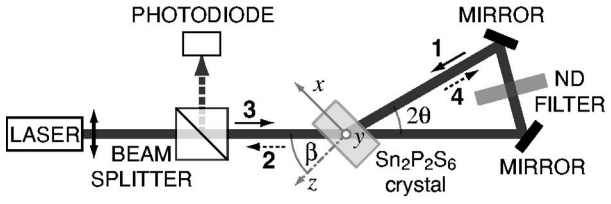

Fig. 4. Experimental setup for the ring-cavity self-pumped phase conjugation with $Sn_2P_2S_6$. Without the external loop, input beam 3 was fanned toward the $+x$ direction. All beams are polarized in the plane of the loop. The transmission grating is written by beam 3 with its self-diffracted beam 4 and by beams 1 and 2 counterpropagating in the loop.

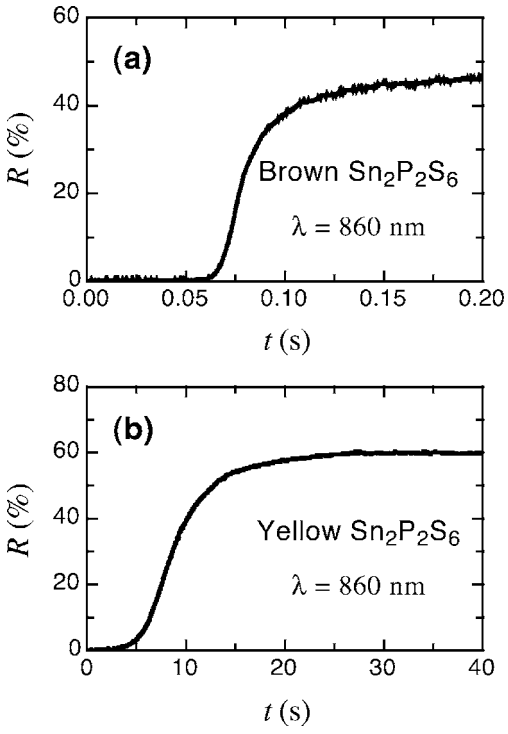

Fig. 5. Time evolution of the phase-conjugate reflectivity R after input beam 3 was turned on using (a) brown $Sn_2P_2S_6$ of 2.4 nm thickness and (b) yellow $Sn_2P_2S_6$ of 9.7 mm thickness. The input beam is at $\lambda=860$ nm and has a diameter of 1.2 mm and powers of (a) 30 mW and (b) 90 mW.

value. We define the reflectivity rise time as the time in which the reflectivity rises from 10% to 90% of its saturation value.

A. Theoretical Background

The measured data for the saturated reflectivity were compared to a plane-wave solution of the coupled equations for the case of large coupling (depleted pump) assuming negligible absorption.[25] The boundary conditions for our ring-cavity self-pumped phase conjugator are $A_1(0)=t_0A_3(0)$, $A_2(0)=t_0A_4(0)$, and $A_4(L)=0$, where $A_i(z)$ is the electric field amplitude of the ith wave at the position z along the propagation, where the position $z=0$ is at the crystal boundary on the side of the ring cavity and $z=L$ is at the input beam boundary. The parameter t_0 accounts for the changes of the beam amplitudes and phases after being reflected by both mirrors in the cavity and being transmitted through the sample surface at $z=0$. The total light intensity is equal to $I_0=|A_1|^2+|A_2|^2+|A_3|^2+|A_4|^2$ and is independent of z if the absorption is neglected. The four coupled-wave equations can be integrated to obtain the solution in the form[25]

$$|t_0|^2\frac{\tanh\kappa L}{s+\sigma\tanh\kappa L}=\frac{s-I_0\tanh\kappa L}{(\sigma I_0-s^2)\tanh\kappa L+(I_0-\sigma)s}, \quad (3)$$

where

$$\sigma=I_0\frac{|t_0|^2-1}{|t_0|^2+1}, \quad (4)$$

$$s=\sqrt{\sigma^2+(I_0-\sigma)^2|\rho|^2}, \quad (5)$$

Table 2. Characteristic Parameters for Phase Conjugation with Brown and Yellow $Sn_2P_2S_6$ Crystals[a]

$Sn_2P_2S_6$ Sample	λ (nm)	α_x (cm^{-1})	I_0 (W/cm^2)	R_0 (%)	τ_0 (s)	Γ (cm^{-1})	T_0 (%)	I_β (W/cm^2)
Brown	633	5.65	0.27	1.8	0.077	36	2.5	0.01±0.005
(L=2.42 mm)	780	0.88	4.0	35	0.011	20	45	0.1±0.05
	860	0.33	2.5	48	0.045	18	62	0.2±0.08
	980	0.14	5.2	35	0.42	14	62	0.3±0.1
Yellow	633	0.49	0.27	23	1.6	6.8	28	0.04±0.02
(L=9.72 mm)	780	0.21	4.0	55	2.4	5.6	62	0.45±0.1
	860	0.16	8.0	60	9.3	4.0	82	1.1±0.3

[a]The given parameters correspond to the experimental results with the crystals of thickness L at different wavelengths λ with maximum input intensities I_0. R_0 is the measured saturated reflectivity and τ_0 is the phase-conjugation rise time. The photorefractive gain Γ and the maximal loop transmission T_0 are the model parameters of Eq. (3) obtained from measurements of reflectivity as a function of loop transmission. The effective background intensity I_β is a model parameter of the dependence of reflectivity on intensity. The relative errors of the parameters I_0, R_0, τ_0, Γ, and T_0 are in the range of 10–20%.

$$\kappa = \frac{s\Gamma^*}{4I_0}, \tag{6}$$

and $|\rho|^2$ is the phase-conjugate reflectivity defined as

$$|\rho|^2 = \left|\frac{A_2(L)}{A_3^*(L)}\right|^2. \tag{7}$$

By inserting Eqs. (4)–(6) into Eq. (3) one obtains the transcendental equation for the reflectivity $|\rho|^2$, which depends on the coupling constant ΓL and $|t_0|^2=T_0$ that we refer to as the loop transmission. The measured reflectivity is equal to $R=|\rho|^2|t_L|^4$ where t_L accounts for the changes of amplitudes and phases of interacting beams after being transmitted through the sample surface at $z=L$.

In the case when absorption is not negligible, the optical energy is not conserved in the crystal and the coupled-wave equation cannot be integrated analytically. Numerical calculations,[26] however, have shown that the absorption can be considered together with the other cavity losses, if the ratio between the linear absorption and the gain α/Γ is less than ~0.1, which is mostly fulfilled in our experimental situations (see Table 2).

B. Loop Transmission Dependence

In addition to the two-beam coupling mechanism and the initial spatial distribution of the incident light, the ring-cavity losses are of crucial importance for the self-pumped phase conjugation. To study the characteristics of the ring-cavity scheme, the cavity transmission was decreased additionally by adding neutral-density (ND) filters into the ring as shown in Fig. 4. The results of the dependence of the saturated reflectivity R on the loop transmission T are shown in Fig. 6 for yellow and brown $Sn_2P_2S_6$ samples at various wavelengths. By decreasing the transmission of the loop, the maximum reflectivity decreases until the threshold is reached. Comparing measured reflectivities with the theoretical reflectivities given by Eq. (3), two crystal parameters can be determined[17]: ΓL, the coupling strength, and T_0, the loop transmission without the ND filter. The theoretical curves in Fig. 6 result in gain values Γ and loop transmissions T_0 as given in Table 2. Higher loop transmission T_0 (and consequently higher phase-conjugate reflectivity) in the yellow sample is a result of lower absorption losses in this crystal. The rise time was not much affected by small additional losses, but increased considerably when approaching the transmission threshold.[17] The obtained gain values Γ (Table 2) can be compared with the values measured by

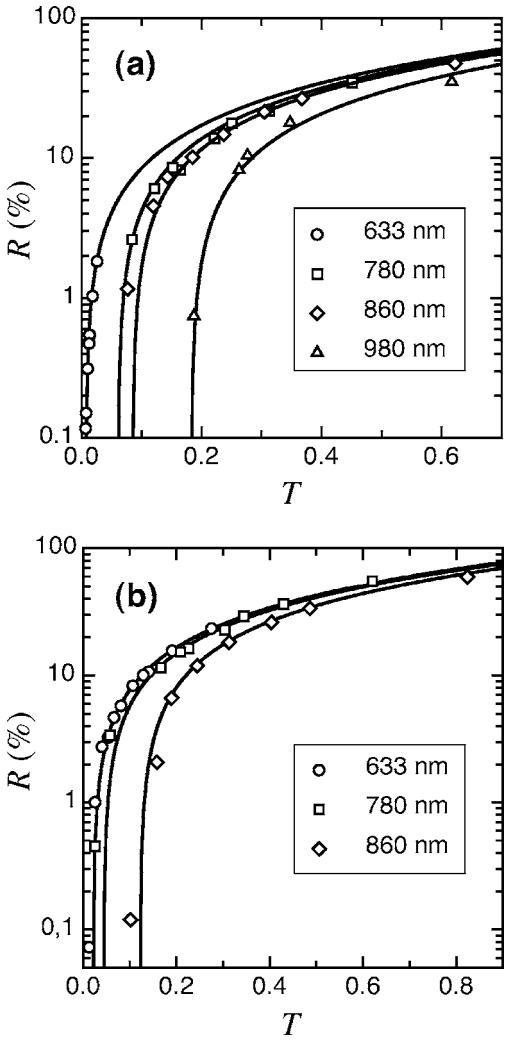

Fig. 6. Measured saturated phase-conjugate reflectivity R as a function of loop transmission T using (a) brown $Sn_2P_2S_6$ of 2.4 mm thickness and (b) yellow $Sn_2P_2S_6$ of 9.7 mm thickness. The solid curves are calculated from Eq. (3) with parameters listed in Table 2, where input beam intensities I_0 for this experiment are also given.

two-wave mixing (Fig. 3). In the yellow sample of 0.97 cm thickness the obtained values from the phase conjugation are approximately twice as high as in the yellow sample of 0.57 cm used in the two-wave mixing experiment. The theory we are using is derived for the plane-wave approximation and is convenient for thin photorefractive crystals without considerable distortion of the beam because of the photorefractive fanning. A slight variation in the properties of the two yellow type II samples used in the experiments is also possible. The obtained values from the two different experiments for the brown sample of 0.24 cm thickness are, on the other hand, in good agreement.

C. Intensity Dependence

Phase-conjugation performance is affected also by the input beam intensity. The response rate increased linearly with intensity in the measured intensity regime as expected for the two-beam coupling time constant.[17] The results of the dependence of the saturated phase-conjugate reflectivity on the input intensity are shown in Fig. 7. The reflectivity increases for lower intensities above some threshold intensity and then it saturates at the maximum value limited by the ring-cavity characteristics. This kind of intensity thresholding was explained with the excitation of carriers due to the thermal effects and by background uniform illumination competing with the spontaneous buildup of the grating. To model the intensity dependence we can take into account the background uniform illumination I_β in the coupled-wave equations, which changes the parameter κ defined in Eq. (6) to

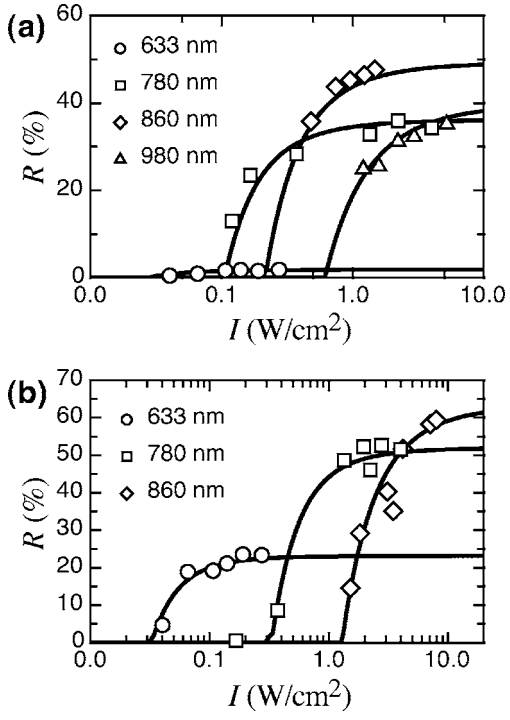

Fig. 7. Measured saturated phase-conjugate reflectivity R as a function of the incident intensity I_3 using (a) brown $Sn_2P_2S_6$ and (b) yellow $Sn_2P_2S_6$. The solid curves are calculated from Eq. (3) considering additional uniform charge generation included in Eq. (8) with parameters ΓL and T_0 as in Fig. 6 and I_β parameters that correspond best to the measured values (see Table 2).

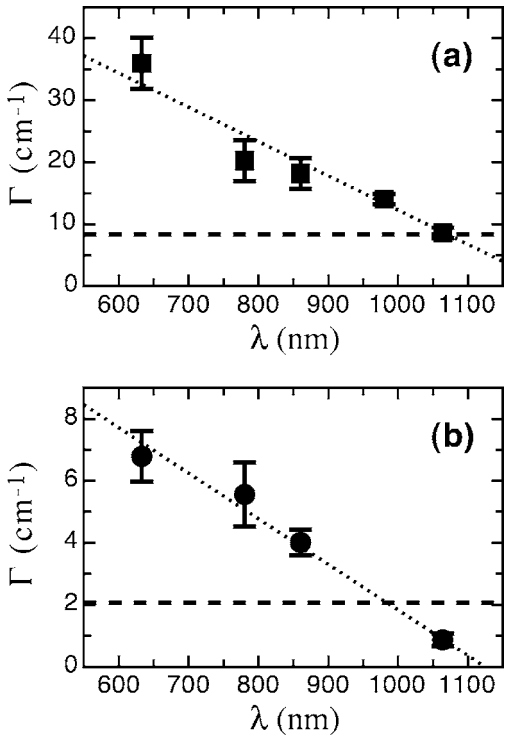

Fig. 8. Photorefractive gain Γ as a function of the light wavelength λ in (a) brown $Sn_2P_2S_6$ and (b) yellow $Sn_2P_2S_6$. The dashed lines correspond to the coupling strength threshold $\Gamma L = 2$ for the brown sample with $L = 2.4$ mm and the yellow sample with $L = 9.7$ mm. The dotted lines present approximations of the dependences $\Gamma(\lambda)$ used to estimate the theoretical limits of the phase-conjugate reflectivities.

$$\kappa = \frac{s\Gamma^*}{4(I_0 + I_\beta)}. \tag{8}$$

The solid curves shown in Fig. 7 represent the intensity dependences of the reflectivity with the previously obtained parameters ΓL and T_0 and the effective background illuminations parameters I_β as listed in Table 2. Since the saturation of the reflectivity is already well reached at the input intensities used for the loop transmission dependence measurements, the curves in Fig. 6 do not change considerably where we take into account I_β. The smaller I_β in the brown sample can be explained by an increased photoconductivity in brown $Sn_2P_2S_6$ compared with conventional yellow $Sn_2P_2S_6$.

D. Dependence of the Phase-Conjugation Response on the Grating Coupling Strength

Figure 8 shows the measured gain Γ in brown and yellow $Sn_2P_2S_6$ versus the light wavelength λ, as obtained from the phase-conjugation experiments (see Table 2) and at $\lambda = 1064$ nm from the two-wave mixing experiments. The dashed lines correspond to the theoretical coupling strength threshold for the ring-cavity self-pumped phase conjugation $\Gamma L = 2$ (Ref. 25) for the brown sample with $L = 2.4$ mm and the yellow sample with $L = 9.7$ mm. For example, at $\lambda = 1064$ nm the gain is at the threshold for the phase-conjugate wave generation in the brown sample; therefore one needs a thicker sample to observe the phase conjugation above this wavelength.

Although the gain is much higher and the phase-conjugate response is much faster in brown $Sn_2P_2S_6$ than in yellow $Sn_2P_2S_6$, the saturated reflectivity was lower in brown $Sn_2P_2S_6$ (see Fig. 5 or Table 2). This was attributed to a lower loop transmission as a consequence of a higher absorption in brown $Sn_2P_2S_6$. Therefore phase-conjugate reflectivities can be higher at longer light wavelengths λ provided that the performance is not yet limited by the coupling strength that decreases with λ. To check whether the reflectivities in the $Sn_2P_2S_6$ samples are also limited by the coupling strength, theoretical dependences of the reflectivity as functions of the coupling strength were plotted in Fig. 9 considering the corresponding loop transmission parameters. Above the coupling strength threshold the reflectivity increases with ΓL until it saturates at a value equal to the transmission of the loop reduced by the reflection losses at the input crystal surface. For the experimental points in Fig. 9 that already reach the saturation, the reflectivity is limited by the loop-cavity transmission and not by the coupling strength. One can conclude that the grating strength started to be a limiting factor for the investigated yellow sample at 860 nm and for the brown sample at 980 nm. At all other measured wavelengths the reflectivity is limited only by the loop-cavity transmission.

E. Optimization of the Phase-Conjugation Performance

From the examples of the loop transmission and the coupling strength threshold shown above, one can conclude

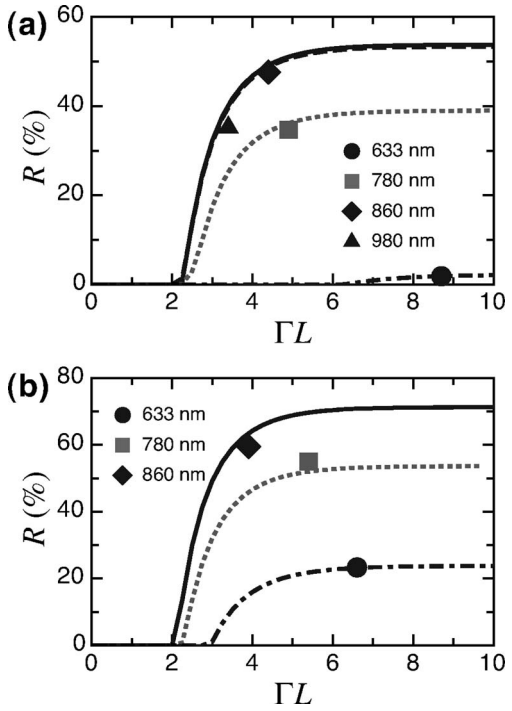

Fig. 9. Theoretical dependences of saturated reflectivity R on the coupling strength for loop transmissions T_0 obtained at different wavelengths (Table 2): 633 nm (dashed–dotted curve), 780 nm (dotted curve), 860 nm (solid curve), 980 nm (dashed curve). Experimental points for (a) brown $Sn_2P_2S_6$ and (b) yellow $Sn_2P_2S_6$ are also included. Note that since the losses at the mirrors inside the cavity were higher at 980 nm but the absorption losses were lower at 980 nm, the curves for brown $Sn_2P_2S_6$ at 980 and 860 nm almost coincide.

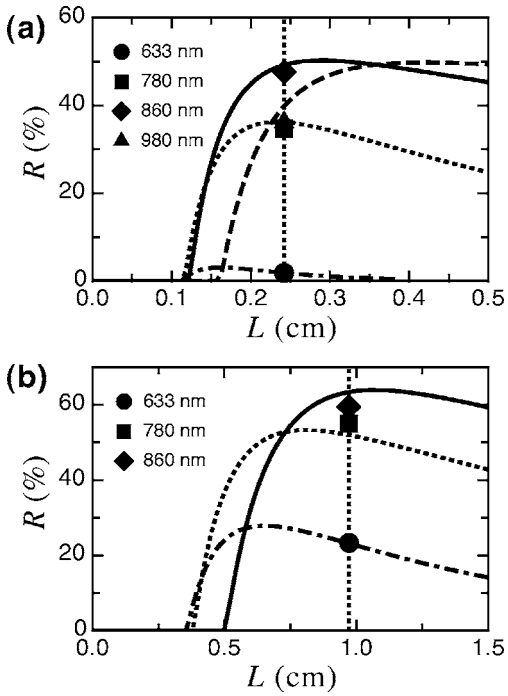

Fig. 10. Theoretical dependences of saturated reflectivity R on the crystal length for loop transmissions T_0, photorefractive gains Γ, and absorption constants α obtained at different wavelengths (Table 2): 633 nm (dashed–dotted curve), 780 nm (dotted curve), 860 nm (solid curve), 980 nm (dashed curve). Experimental points for (a) brown $Sn_2P_2S_6$ and (b) yellow $Sn_2P_2S_6$ are also included with the dotted vertical lines corresponding to the investigated crystal thicknesses.

that there exists an optimal crystal thickness for the ring-cavity self-pumped phase conjugation at each wavelength. If the reflectivity is limited by the coupling strength, using a thicker crystal could result in a better performance. If it is limited by the cavity transmission, it could be advantageous to use a thinner crystal. Figure 10 shows the calculated phase-conjugate reflectivities as functions of the crystal length considering the parameters listed in Table 2. At each wavelength there is a maximum in the phase-conjugate reflectivity that corresponds to the optimal crystal length. The dotted vertical lines correspond to the brown and yellow crystals investigated. One can conclude that both are of the optimal thickness for wavelengths of ~860 nm. For shorter wavelengths it will be advantageous to use thinner crystals, for longer wavelengths thicker ones. Selecting a crystal according to the maximum reflectivity presented in Fig. 10 will assure the lowest possible absorption losses without starting to limit the reflectivity due to the coupling strength. Such a crystal can then be antireflection coated for a selected wavelength, minimizing the reflection losses at the crystal surface.

Considering the above optimization procedure, we have calculated the optimal reflectivities as functions of the wavelength for yellow and brown $Sn_2P_2S_6$. For this purpose we have approximated the dependences $\Gamma(\lambda)$ presented in Fig. 8 with linear functions. Such linear dependences have no physical meaning; we use them only as first approximations for our calculation. We assume further only absorption losses; therefore the loop transmis-

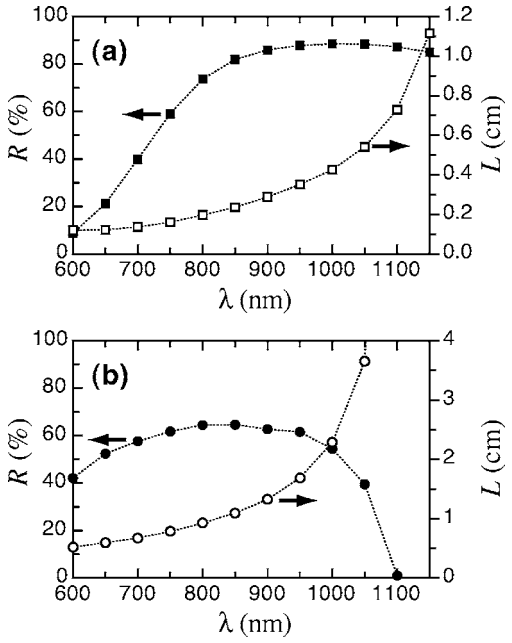

Fig. 11. Optimized phase-conjugate reflectivity R (left scale) as a function of the light wavelength λ for (a) brown $Sn_2P_2S_6$ and (b) yellow $Sn_2P_2S_6$ crystal of the optimal thickness L (right scale).

sion parameter is $T_0=\exp(-2\alpha L)$, where the absorption constant values α are plotted in Fig. 2. At each light wavelength λ we can then calculate the dependence of the saturated reflectivity R as a function of the crystal thickness L, similar as in Fig. 10. Figure 11 shows the dependence of the reflectivity maximum and the crystal length at the maximum as a function of λ. In optimized crystals, reflectivities up to ~90% are possible using brown $Sn_2P_2S_6$ and up to ~65% using yellow $Sn_2P_2S_6$. The optimal wavelength range for brown $Sn_2P_2S_6$ is 850–1100 nm with crystals 0.25–0.7 cm thick. The optimal wavelength range for yellow $Sn_2P_2S_6$ is 650–950 nm with crystals 0.6–1.7 cm thick.

5. CONCLUSIONS

Photorefractive properties and self-pumped phase conjugation in yellow and brown $Sn_2P_2S_6$ crystals were studied in the near-infrared wavelength range. Compared with the most popular photorefractive material for the near-infrared applications, Rh-doped $BaTiO_3$, $Sn_2P_2S_6$ crystals are especially advantageous because of the dynamic response, which is typically 2 orders of magnitude faster. The photorefractive gain in the near infrared, 18 cm^{-1} at 780 nm and 8.5 cm^{-1} at 1064 nm, is high enough to allow many potential applications. We are especially interested in applying phase conjugation in the near infrared. Thresholding behavior regarding the ring-cavity transmission, light intensity, and photorefractive coupling strength for the ring-cavity self-pumped phase conjugation was investigated in detail. The presented analysis allows us to optimize the phase-conjugation performance. The optimal wavelength range for yellow $Sn_2P_2S_6$ is 650–950 nm and for brown $Sn_2P_2S_6$ it is 850–1100 nm with optimal phase-conjugate reflectivities of up to 90%. In addition to optimizing the available yellow and brown $Sn_2P_2S_6$ crystals of different stoichiometry levels, we are also looking for new crystal modifications with dopants to further improve the photorefractive performance of $Sn_2P_2S_6$.

ACKNOWLEDGMENTS

This research has been supported by the Swiss National Science Foundation.

The present address for G. Montemezzani is Laboratoire Matériaux Optiques, Photonique et Systemès (Unité Mixte de Recherche, Centre National de la Recherche Scientifique 7132), University of Metz and Supélec, 57070 Metz, France.

REFERENCES

1. P. Günter and J.-P. Huignard, eds., *Photorefractive Materials and their Applications I and II* (Springer-Verlag, 1988).
2. P. Yeh, *Introduction to Photorefractive Nonlinear Optics* (Wiley, 1993).
3. G. Montemezzani, C. Medrano, M. Zgonik, and P. Günter, "The photorefractive effect in inorganic and organic materials," in *Nonlinear Optical Effects and Materials*, Vol. 72 of Springer Series in Optical Science, P. Günter, ed. (Springer, 2000), pp. 301–373.
4. M. Ewart, R. Ryf, C. Medrano, H. Wüest, M. Zgonik, and P. Günter, "High photorefractive sensitivity at 860 nm in reduced rhodium-doped $KNbO_3$," Opt. Lett. **22**, 781–783 (1997).
5. G. W. Ross, P. Hribek, R. W. Eason, M. H. Garrett, and D. Rytz, "Impurity enhanced self-pumped phase conjugation in the near-infrared in 'blue' $BaTiO_3$," Opt. Commun. **101**, 60–64 (1993).
6. N. Huot, J. M. C. Jonathan, G. Pauliat, D. Rytz, and G. Roosen, "Characterization of a photorefractive rhodium doped barium titanate at 1.06 μm," Opt. Commun. **135**, 133–137 (1997).
7. M. Kaczmarek, R. W. Eason, and I. Mnushkina, "The effect of doping and processing conditions on the optical performance of Rh:$BaTiO_3$," Appl. Phys. B **68**, 813–817 (1999).
8. N. Huot, J. M. C. Jonathan, G. Roosen, and D. Rytz, "Characterization and optimization of a ring self-pumped phase conjugate mirror at 1.06 μm with $BaTiO_3$:Rh," J. Opt. Soc. Am. B **15**, 1992–1999 (1998).
9. A. Shumelyuk, D. Barilov, S. Odoulov, and E. Krätzig, "Anisotropy of the dielectric permittivity of $Sn_2P_2S_6$ measured with light-induced grating techniques," Appl. Phys. B **76**, 417–421 (2003).
10. A. Shumelyuk, S. Odoulov, and G. Brost, "Multiline coherent oscillation in photorefractive crystals with two species of movable carriers," Appl. Phys. B **68**, 959–966 (1999).
11. S. G. Odoulov, A. N. Shumelyuk, U. Hellwig, R. A. Rupp, and A. A. Grabar, "Photorefractive beam coupling in tin hypothiodiphosphate in the near infrared," Opt. Lett. **21**, 752–754 (1996).
12. S. G. Odoulov, A. N. Shumelyuk, U. Hellwig, R. A. Rupp, A. A. Grabar, and I. M. Stoika, "Photorefraction in tin hypothiodiphosphate in the near infrared," J. Opt. Soc. Am. B **13**, 2352–2360 (1996).
13. A. Shumelyuk, S. Odoulov, and G. Brost, "Electric-field enhancement of beam coupling in $Sn_2P_2S_6$," Appl. Phys. B **72**, 707–710 (2001).
14. A. Shumelyuk, S. Odoulov, and G. Brost, "Nearly degenerate two-beam coupling in photorefractive crystals with two species of movable carriers," J. Opt. Soc. Am. B **15**, 2125–2131 (1998).
15. A. Shumelyuk, S. Odoulov, H. Yi, E. Krätzig, and G. Brost,

"Ti-sapphire laser beam coupling in $Sn_2P_2S_6$," in *Conference on Laser and Electro-Optics*, Vol. 6 of OSA Technical Digest Series (Optical Society of America, 1998), pp. 171–172.
16. A. A. Grabar, I. V. Kedyk, M. I. Gurzan, I. M. Stoika, A. A. Molnar, and Yu. M. Vysochanskii, "Enhanced photorefractive properties of modified $Sn_2P_2S_6$," Opt. Commun. **188**, 187–194 (2001).
17. M. Jazbinšek, G. Montemezzani, P. Günter, A. A. Grabar, I. M. Stoika, and Yu. M. Vysochanskii, "Fast near-infrared self-pumped phase conjugation with photorefractive $Sn_2P_2S_6$," J. Opt. Soc. Am. B **20**, 1241–1246 (2003).
18. C. D. Carpentier and R. Nitsche, "Vapor growth and crystal data of thio(seleno)-hypodiphosphates $Sn_2P_2S_6$, $Sn_2P_2Se_6$, $Pb_2P_2S_6$, $Pb_2P_2Se_6$ and their mixed crystals," Mater. Res. Bull. **9**, 401–410 (1974).
19. D. Haertle, A. Guarino, J. Hajfler, G. Montemezzani, and P. Günter, "Refractive indices of $Sn_2P_2S_6$ at visible and infrared wavelengths," Opt. Express **13**, 2047–2057 (2005).
20. R. S. Cudney, R. M. Pierce, G. D. Bacher, and J. Feinberg, "Absorption gratings in photorefractive crystals with multiple levels," J. Opt. Soc. Am. B **8**, 1326–1332 (1991).
21. D. Haertle, G. Caimi, A. Haldi, G. Montemezzani, P. Günter, A. A. Grabar, I. M. Stoika, and Yu. M. Vysochanskii, "Electro-optic properties of $Sn_2P_2S_6$," Opt. Commun. **215**, 333–343 (2003).
22. N. V. Kukhtarev, V. B. Markov, S. G. Odoulov, M. S. Soskin, and V. L. Vinetskii, "Holographic storage in electrooptic crystals 2. Beam coupling-light amplification," Ferroelectrics **22**, 961–964 (1979).
23. G. Montemezzani and M. Zgonik, "Light diffraction at mixed phase and absorption gratings in anisotropic media for arbitrary geometries," Phys. Rev. E **55**, 1035–1047 (1997).
24. P. Günter and M. Zgonik, "Clamped–unclamped electro-optic coefficient dilemma in photorefractive phenomena," Opt. Lett. **16**, 1826–1828 (1991).
25. M. Cronin-Golomb, B. Fischer, J. O. White, and A. Yariv, "Theory and applications of four-wave mixing in photorefractive media," IEEE J. Quantum Electron. **QE-20**, 12–30 (1984).
26. J. E. Millerd, E. M. Garmire, and M. B. Klein, "Investigation of photorefractive self-pumped phase-conjugate mirrors in the presence of loss and high modulation depth," J. Opt. Soc. Am. B **9**, 1499–1506 (1992).